NASA
Technical
Paper
2175

June 1983

Elastohydrodynamic Contacts

Effects of Dents and Grooves on Traction and Local Film Thickness

Lavern D. Wedeven
and Cristino Cusano

NASA

25th Anniversary
1958-1983

NASA
Technical
Paper
2175

1983

Elastohydrodynamic Contacts

Effects of Dents and Grooves on Traction and Local Film Thickness

Lavern D. Wedeven
Lewis Research Center
Cleveland, Ohio

Cristino Cusano
University of Illinois at Urbana-Champaign
Urbana, Illinois

National Aeronautics
and Space Administration

**Scientific and Technical
Information Branch**

Summary

Traction and film thickness were simultaneously measured under sliding elastohydrodynamic (EHD) point-contact conditions as surface defects in the form of shallow dents and grooves were positioned in or near the contact region. The experiments were run under a constant load (38.3 N) at a maximum Hertzian pressure of 1.13 GPa (163 000 psi) and two sliding velocities (0.037 and 0.107 m/s), giving two nominal film thicknesses of 0.16 and 0.26 μm.

With a synthetic paraffinic oil as the lubricant, surface defects increased the traction coefficient of the order of 25 percent. Transversely oriented grooves increased traction to a greater degree than longitudinal grooves. When dents were located in the inlet region, where the film thickness is generated, traction could be enhanced or diminished depending on whether the defect topograph improved or degenerated film thickness in the contact region. Observations of local surface deformation made with interferometry showed that the enhancement of traction was caused by micro-EHD pressure generation associated with the converging portions of the defect topography. The results imply the possibility of improving the traction capacity of lubricated contacts with appropriate surface topographical structure without intimate mechanical interaction between asperities. Locally high normal and shear stresses are likely to be present. It is postulated that the asperity environment created by the micro-EHD action can be involved in the process of "run-in" or the initiation of surface failure.

Introduction

The life and reliability of many aerospace components such as gears, bearings, and traction drive elements depend on the lubrication of the intimate concentrated-contact areas that carry the load and bear the shear between the surfaces. Because some sliding occurs in essentially all concentrated contacts, these contacts are generally subjected to conditions that are more severe than pure rolling conditions. This leads to a greater probability of surface failure initiation. The presence of sliding in elastohydrodynamic (EHD) contacts not only results in frictional heat generation and possible heat-associated contact failures, but also produces tangential forces that influence both fatigue and skidding failures in rolling-element bearings. Involved in this is the probability of micro-EHD action associated with irregularities on the contacting surfaces (refs. 1 to 3). That is, the generation of pressure and film thickness on an asperity scale. This action can change locally the film thickness and pressure distribution and can be expected to influence the traction as well.

The traction coefficient (ratio of traction force to normal load) is associated with the energy dissipation in a lubricated contact and is freqently correlated with surface failure. In addition, the traction coefficient is intimately associated with the design and performance of traction drives. Hewko et al. (ref. 4) found that tractive capacity can be significantly influenced by surface topography. For reasons of surface durability and life it is of interest to know the degree to which the tractive capacity can be enhanced by a purely hydrodynamic (or micro-EHD) effect as opposed to what may loosely be called direct mechanical interaction of asperities. Most traction measurements have been made under full-film EHD conditions, that is, where surface roughness is expected to be of secondary significance (refs. 5 and 6). Since it is widely recognized that in practice most mechanical elements do not continuously operate under such ideal conditions, there have been recent efforts to more fully understand the role surface topography plays in traction developed in EHD contacts (refs. 7 to 9).

The present work reports on the effects of surface irregularities, in the form of dents and grooves, on traction in sliding EHD point contacts and correlates the measured traction changes with local film thickness changes. In previous investigations (refs. 1 to 3) it was noted that these surface irregularities could cause large film thickness variations near the irregularities as well as throughout the contact. From these film thickness changes it can be inferred that traction could also change. Many of the traction measurements reported herein were taken under similar conditions to the film thickness measurements of reference 3. Even though an exhaustive experimental program has not been conducted, the results presented herein give some indication as to traction changes caused by surface irregularities as these irregularities are located progressively through the contact. As in previous investigations (refs. 1 to 3) the contact was formed by a ball loaded against a transparent disk. The irregularities or defects were formed on the ball and held stationary at various positions in the inlet and Hertzian regions while the disk was moving. Film thickness and traction were monitored simultaneously. Because of the experimental difficulties involved in the simultaneous measurements of film thickness and traction of isolated defects, only one kinematic condition (i.e., stationary defects and smooth surface moving) was investigated. This is only one of the many possible kinematic conditions to be found in practice.

Symbols

a	radius of Hertzian contact
C	dimensionless defect width, $C=c/a$
c	one-half of largest width of single dent or groove or average of largest widths of multiple grooves
F	traction force
F_0	traction force for smooth surfaces
h	film thickness
h_0	central film thickness based on smooth surfaces
u	sliding velocity (velocity of smooth surface)
X	dimensionless defect position, $x=x/a$
x	distance from center of Hertzian contact to center (deepest part) of dent or transverse groove or to center (deepest part) of groove closest to contact for multiple transverse grooves
Δ	dimensionless defect depth, $\Delta=\delta/h_0$
δ	maximum depth of single defects or average maximum depth of multiple defects
φ_d	characteristic slope of defect, $\varphi_d=\arctan \delta/c$
σ	average surface roughness height

Experimental Apparatus

Both traction and film thickness were measured by using the optical elastohydrodynamic apparatus shown in figure 1. This apparatus is described in detail elsewhere (refs. 10 and 11), but the procedure for both traction and film thickness measurements is described briefly herein. The traction between the ball and the disk was obtained by measuring the reaction force on the ball. The test ball drive, gear reducer, and load cylinder shown in figure 1 were suspended on an air bearing that pivoted at one end and was restrained at the other end by springs. The reaction force on the ball was directly proportional to the deflection of the springs. This deflection was measured by means of a capacitance transducer.

Film thickness was measured by means of optical interferometry. Fringes of very good visibility were obtained by using a 17-percent-reflecting layer of chromium on the bearing surface of the transparent disk. Interference was measured with wavelengths of two colors (red and green). These were obtained by using a special filter and a xenon flash lamp as a light source. The details of this system and its calibration are described more fully in references 12 and 13. All measurements were made at room temperature.

Test Materials

The test ball was 0.02063 m in diameter and made of AISI 52100 steel. Its nominal surface roughness was 0.018 μm rms (0.7 μin.) and its hardness was approximately 65 R_c. Its Other mechanical properties are given in table I. The transparent disk was 0.102 m in diameter and made of sapphire. Its mechnical properties are also given in table I.

The test ball was supported by three bearings located in a lubricant reservoir shown in figure 1. The formation of the artificial defects on the ball is described in detail in reference 1. Tests were performed with a synthetic paraffinic oil whose properties are given in table II.

Procedure

The surface defects were positioned at various locations in the conjunction region, and traction data were taken at each location. At the same time single-flash photographs were taken of the contact to determine the film thickness variations, particularly downstream of the defects, as done in reference 3. Stylus traces through the deepest part of the "undeformed" defects were taken after the testing program. The experiments were run at room temperature. A load of 38.3 N was used, giving a maximum Hertzian pessure of 1.13 GPa (163 000 psi). Two sliding velocities were used (0.037 and 0.107 m/s) corresponding to two central film thicknesses (0.16 and 0.26 μm). With smooth surfaces these two velocities gave coefficients of traction of 0.064 and 0.061, respectively.

The variables used to describe the geometry of the defects as well as their position relative to the contact region are shown in figure 2. Three dimensionless parameters were used to specify the geometry and position of the defects. The position is specified by $X=x/a$, where x is the distance from the center of the Hertzian contact to the center (deepest part) of the dent or the single transverse groove or the distance to the center (deepest part) of the groove closest to the contact for multiple transverse grooves and a is the contact radius. The width of the defects is specified by $C=c/a$, where c is one-half of the largest width of a single defect or one-half of the average of the largest widths of multiple transverse grooves. The normalized depth of the defects is specified by the parameter $\Delta=\delta/h_0$, where δ is the maximum depth of a single defect or the average maximum depth of multiple transverse grooves and h_0 is the central film thickness based on smooth surfaces. Because most of the defects have built-up edges, the

TABLE I. - TEST BALL AND DISK MATERIAL PROPERTIES

	Ball	Disk
Material	52100 Steel	Sapphire
Compressive strength, N/m^2	1.4×10^9	2×10^9
Elastic modulus, N/m^2	204×10^9	365×10^9
Poisson's ratio	0.3	0.25
Hardness	65 R_C	9 Moh
Roughness, μm rms	0.018	Optical polish

TABLE II. - TEST FLUID PROPERTIES

[Test fluid, synthetic paraffinic oil (XRM 109F3).]

Viscosity, cS:	
At -17.8° C	45 830
At 37.8° C	493
At 98.9° C	42.6
Density, g/cm^3:	
At 37.8° C	0.8389
At 93.3° C	0.8082
At 149° C	0.777
Pressure-viscosity coefficient, m^2/N:	
At 37.8° C	1.77×10^{-8}
At 99° C	1.51×10^{-8}
At 149° C	1.09×10^{-8}
Refractive index at 23° C	1.4689

values of c and δ were obtained by extending the smooth-surface profile on both sides of the defects, as shown in figure 3. Also note from figure 3 that in approximating the value of c, the rounded edges (left side of dent) were not considered. Measurements from five types of defects are presented herein. These include a small dent, a large dent, a transverse groove, a longitudinal groove, and a series of three parallel transverse grooves. The dimensions δ and c for the various surface defects are shown in table III. Also shown in table III is the characteristic slope φ_d of the defects defined as

$$\varphi_d = \arctan \delta/C$$

Note that the values of φ_d range from slightly less than 1° to slightly more than 2°, indicating the very shallow characteristic of the defects. The widths of the defects are of the order of one hundred times greater than their depth.

Results with a Single Dent

Traction and film thickness were measured for a surface with a small dent (fig. 3) and a larger dent (fig. 4). These data were obtained at a nominal film thickness h_0 of 0.26 μm. The maximum Hertzian pressure was 1.13 GPa, giving a Hertzian contact radius a of 127 μm. The values of Δ and C were 3.9 and 0.45, respectively, for the small dent and 6.0 and 0.49 for the larger dent. Traction and film thickness were measured for both dents as a function of their location in and near the contact region. The influence of dent location on film thickness was measured by interferometry. Photomicrographs of the interference fringes used to obtain the film thickness data are shown in figure 5 for the small dent. Under sliding conditions with the dent stationary, film thickness increased significantly downstream of the dent. Relative traction F/F_0 and film thickness h/h_0 as a function of dent position are shown in figure 6. Both traction and film thickness were normalized with respect to their smooth-surface values represented by the zero subscript.

The presence of surface dents generally gave a traction force that was above that obtained for smooth surfaces (fig. 6(a)). A transition from higher to lower traction occurred when the dents were located at the leading edge of the Hertzian region ($X \simeq 1$). The dents in this position changed the shape of the inlet region and enhanced the generation of inlet pressure, as implied by the film thickness data given in figure 6(b). With the dents located near $X = 1$, the film thickness downstream of the dents was much larger than the film thickness based on smooth surfaces. With such large increases in downstream film thickness, the traction force was less than the smooth-surface value, as indicated in figure 6(a) for the small dent. However, with dents positioned at any other location near the inlet and inside the contact, the traction was higher than the smooth-surface value even though, at some points, the downstream film thickness was greater than the corresponding smooth-surface value. The

TABLE III. - SURFACE DEFECT DIMENSIONS

Defect	Maximum depth of single defect or average for multiple defects, δ, μm	One-half of widest single defect or average width of widest multiple grooves, c, μm	Characteristic slope of defect action δ/c, φ_d, deg
Small dent	1.01	57.2	1.0
Large dent	1.56	62.2	1.5
Transverse groove	.40	25.0	.92
Longitudinal groove	.70	19.1	2.1
Three parallel transverse grooves (average)	.42	17.8	1.3

enhancement in traction appeared to be associated with local micro-EHD action near the dent, giving rise to local pressures that can be much higher than the pressure generated with smooth surfaces. Figure 6 shows that the enhancement in traction was greater for the larger dent.

Results with a Single Groove

Traction and film thickness were also measured for single grooves oriented both perpendicular and parallel to the sliding motion. A relatively shallow transverse groove is shown in figure 7. Relative traction F/F_0 and film thickness h/h_0 measurements were made for two nominal film thicknesses h_0 (0.16 and 0.26 μm). Figure 8 shows the change in interference pattern for a nominal film thickness (i.e., h_0 for a smooth surface) of 0.16 μm, as the groove was progressively located in different positions relative to the contact region. Note the presence of a dark fringe throughout the contact region in figure 8(b) that is associated with the groove positioned in the inlet region. This dark fringe corresponds to a film thickness reduction of 38 percent ($h = 0.10$ μm). The film thickness and traction data are presented in figure 9. For this relatively shallow groove the film thickness downstream of the groove was equal to or less than the smooth-surface value; the traction was always higher than the smooth-surface value. The transition in traction and film thickness when the groove was in the inlet region ($X \simeq 1$) was not as apparent with this shallow groove as with the dent (fig. 6). There are probably not enough data points around $X \simeq 1$ to clearly define this transition.

Another single groove, but oriented parallel (longitudinally) to the surface motion, is shown in figure 10. Traction was measured at a nominal film thickness of 0.26 μm. The values of C and Δ were 0.15 and 2.7, respectively. The maximum relative traction measured for the longitudinal groove was 1.03. This was less than that for the transverse groove. Even though the two grooves did not have the same geometry, it can generally be stated that, under the same operating conditions, transverse grooves enhanced the traction more than longitudinal grooves did. The difference can be explained by the fact that with the longitudinal groove the micro-EHD contribution to traction was less because the variation in surface profile was predominately parallel to the fluid flow rather than perpendicular to it as with the transverse groove. The interference pattern is compared with the transverse and longitudinal grooves at a nominal film thickness of 0.26 μm in figure 11. The light fringe adjacent to the longitudinal groove (fig. 11(a)) indicates a relatively thin film ($h = 0.16$ μm). The film thickness over the general contact region was less than the smooth-surface value. The local pressure associated with the groove shoulders was likely to be much lower than that for the transverse groove (fig. 11(b)). The interference fringes just upstream of the transverse groove, as well as those on the downstream side of the groove, indicated a local enhancement in film thickness due to the micro-EHD action associated with the groove. These local film thickness alterations are shown in figure 12. Alterations in elastic deformation must be accompanied by substantial pressures and pressure gradients, which are instrumental in enhancing the traction.

Results with Multiple Grooves

In addition to single-groove measurements traction and film thickness were measured with multiple grooves oriented perpendicular to the surface motion. A photomicrograph of three grooves and the surface profile trace are shown in figure 13. Measurements were taken at the two nominal film thicknesses. The average value of C for these grooves was 0.14; the average value of Δ was 2.6 for $h_0 = 0.16$ μm and 1.6 for $h_0 = 0.26$ μm. The interference patterns as these three grooves were progressively positioned through the contact are shown in figure 14. The traction and downstream film thickness data for the various groove positions are shown in figure 15. As with the single transverse groove the film thickness was always less, as the grooves entered and went through the contact,

than the film thickness based on smooth surfaces. The increase in relative traction F/F_0 with the three grooves (fig. 15(a)) was much larger than that for the single groove described previously. The opportunity for micro-EHD pressure enhancement was greater with multiple grooves.

Discussion

The main purpose of this report is to show the influence of micro-EHD effects associated with surface irregularities such as dents and grooves on the traction in sliding EHD point contacts. It was shown that relatively small surface irregularities whose average depth is of the order of 0.4 μm and whose characteristic slope is around 1° or 2° can increase traction beyond the smooth-surface value by 20 to 25 percent. These changes appear to be significant in connection with mechanical components whose performance depends on thin-film traction and lubrication. The increase in traction along with the observation of substantial local micro-EHD film thickness changes implies very high local pressure and pressure gradients associated with the surface irregularities. Its connection with near-surface plastic flow, crack initiation, and surface failure may be significant. Although micro-EHD films are generated to provide asperity separation, the local normal and tangential stresses can still be quite high.

Grooves oriented transversely or longitudinally to the direction of flow increased traction relative to the smooth-surface value under the same operating conditions. The increase was greater for transverse grooves than for longitudinal grooves. Such trends have also been observed in hydrodyhamic lubrication (ref. 14). On the other hand, dents decreased traction for a given operating condition relative to the smooth-surface value. This occurred when the dents were positioned in the inlet region. This decrease was caused by a large local film thickness increase in the contact region as a result of favorable modification of the inlet shape. However, the decrease in traction tended to be relatively small, and it occurred only when the dents were positioned over a small portion of the contact in the inlet region. Over the rest of the contact, traction was greater than the smooth-surface value.

The three grooves shown in figure 13 have an average depth (measured from the smooth surface) of approximately 0.42 μm. Because of their close spacing two adjacent grooves produced a build-up of material (summit) between the grooves. The left summit in figure 13 was approximately 0.1 μm high; the right summit was approximately 0.2 μm high. The average spacing of the summits was 44 μm; the average characteristic slope was 1.30°. The surface topography produced by these three grooves was not substantially different from the fundamental roughness that can be found in some conventionally produced surfaces (ref. 15). A ground surface taken from reference 16 is compared with these grooves in figure 16. Since the horizontal scale was about the same, the main structure (waviness) of the ground surface (indicated by a dashed line) was approximately the same as that of the three grooves. The ground surface was actually "rougher" ($\sigma = 0.5$ μm rms) than the grooved surface ($\sigma = 0.2$ μm rms). In addition, since the central film thicknesses (based on smooth surfaces) of 0.16 and 0.26 μm were approximately the same as the summit heights, the lubrication conditions analyzed for these artificially produced surfaces were likely to be similar to at least some cases found in practice. Therefore the traction data presented for the three grooves should give a good indication of the difference between traction produced by real rough surfaces with approximately the same fundamental roughness and traction based on smooth surfaces if the operating conditions are approximately the same.

The changes in traction from the smooth-surface value can be considered to be composed of two components. One of these components resulted from changes in the inlet surface geometry as the dents and grooves approached the inlet region. Such changes led to lower or higher inlet pressure and greater or lesser film thickness depending on the position of the defects and their geometry. These variations of inlet pressure could raise or lower the central film thickness, giving rise to a corresponding change in traction. The effect was very similar to that observed for the influence of starvation on traction (ref. 10). Both a change in inlet lubricant supply and a change in inlet shape inhibited the generation of hydrodynamic pressure. This resulted in a lower overall film thickness and an effective increase in shear rate, giving rise to an increase in traction. For a severely starved film the traction increased 40 percent while the apparent shear rate u/h_0 increased an order of magnitude (ref. 10).

The second component resulted from micro-EHD pressure generation when the defects were in the Hertzian region. This micro-EHD action redistributed the pressure so that the load was mainly supported by the converging regions of the defects. This implies higher local pressure, temperature, and shear in these local regions. It is postulated that these local pressures can become high enough to cause local asperity plastic flow even without intimate mechanical contact. Although local plastic flow was not observed, the elastic deformations can become quite significant as shown in references 2 and 3. These local deformations along with the observed increase in traction associated with the surface defects imply the existence of substantial normal and shear stresses at the defect sites. These local stresses tended to diminish as the overall film thickness increased. One was left with the view that, as the film thickness decreased, the energy

dissipation became concentrated at asperity sites. It is conceivable that the local temperatures at these sites can promote lubricant-metal chemical action. These local events are likely to be involved in the process of "run in" or surface failure originating on an asperity scale.

The detrimental effect that traction has on fatigue life, particularly for traction drive elements, has caused considerable concern. A fatigue spall can be formed by the initiation of a subsurface or surface crack. A recent analysis based on smooth surfaces (ref. 17) has shown that traction has very little effect on the subsurface shearing stress that would give rise to the classical subsurface-initiated fatigue. The detrimental effect of traction on fatigue may be associated more with surface-initiated cracks derived in the near-surface region from the local tangential stresses at asperity sites. The importance of the film thickness–surface roughness ratio and the role of surface defects in the fatigue of rolling elements have been well established. They would seem to be even more important in the presence of traction.

It is well known that traction in lubricated contacts under EHD conditions is very much a function of the rheological properties of the lubricant. The substantial rise in pressure that the lubricant experiences as it enters the contact region results in an exponential increase in viscosity. Under typical EHD conditions, like those found in these experiments, the lubricant can become an amorphous solid in the high-pressure region of the contact. The traction is then derived from the viscous-elastic-plastic properties of the lubricant as described in references 18 to 20. The transition from liquid to solid behavior is a function of temperature, pressure, and shear rate. For smooth surfaces and the sliding conditions used herein the measured traction coefficients of 0.064 (at 0.037 m/s) and 0.061 (at 0.107 m/s) are expected to be controlled primarily by the limiting shear stress of the lubricant in its amorphous state and at the controlling pressures and temperatures in the contact zone. As shown in reference 18 the limiting shear stress is a linearly increasing function of pressure and a linearly decreasing function of temperature. When surface defects are present in the contact region, the local fluid rheology is expected to influence the tangential stress. It is noted, for example, in figure 6(a) that the measured traction reached a maximum when the dent was in the center of the contact region, where the pressure and limiting shear stress are high.

The presence of local surface defects along with the local micro-EHD deformations observed at the shoulders of the defects must lead to substantial local pressure, temperature, and shear rate variations. These variations of environmental conditions will determine the degree of viscous, elastic, or plastic behavior of the lubricant. The effect of the local rheological behavior is expected to influence the local shear stress at defect sites as well as the ability to generate micro-EHD films. If the lubricant has already reached its shear limit, its ability to provide additional micro-EHD pressure generation may be inhibited. A failure theory based on this type of asperity lubrication postulate has been studied in reference 21. The data in reference 18 show a significant difference in rheological properties, like limiting shear stress, for a variety of lubricants. It would be of interest to study micro-EHD lubrication and traction as a function of lubricant type. From the micro-EHD deformations measured in figure 15 of reference 3, there is some evidence that the synthetic paraffinic oil used herein can generate additional micro-EHD pressure for asperity lubrication. This may not be the case for a fluid such as a dimethylsiloxane, which has a much lower limiting shear strength, as shown in reference 18.

Conclusions

Traction and local film thickness were measured simultaneously under elastohydrodynamic (EHD) sliding conditions as surface defects such as shallow dents and grooves were positioned in and near the contact region. The following conclusions were drawn as a result of this study:

1. With appropriate surface topography it is possible to improve the traction capacity of lubricated contacts without intimate mechanical asperity interaction. With both transverse and longitudinal grooves, the traction increases relative to the smooth-surface value as these defects enter and go through the contacts. Increases are greater with transverse grooves than with longitudinal grooves.

2. With transverse grooves having an average peak-to-peak height of approximately 0.4 μm and a characteristic slope of 1.3°, traction is as much as 20 to 25 percent greater than the smooth-surface value.

3. With dents, traction is lower than the smooth-surface value when the defects are appropriately positioned in the inlet region to provide a more favorable inlet shape, which generates a larger film thickness.

4. When a surface defect, positioned in the inlet region, causes an unfavorable inlet shape, a thinner film is generated and the traction increases in a manner similar to that found under oil starvation conditions.

5. The enhancement of traction with surface defects appears to be due to the micro-EHD pressure generation associated with the converging regions of the defect topography. Although the local pressure, temperature, and lubricant rheological properties are not

quantitatively known, the measured traction and the observation of significant deformations at the defect sites indicate substantial normal and shear stress on a local scale. It is postulated that the local stress and micro-EHD film generation can influence the onset of surface-initiated failure.

Lewis Research Center
National Aeronautics and Space Administration
Cleveland, Ohio, February 8, 1983

References

1. Wedeven, L. D.; and Cusano, C.: Elastohydrodynamic Film Thickness Measurements of Artificially Produced Surface Dents and Grooves. ASLE Trans., vol. 22, no. 4, 1979, pp. 369-381.
2. Cusano, C.; and Wedeven, L. D.: Elastohydrodynamic Film Thickness Measurements of Artificially Produced Nonsmooth Surfaces. ASLE Trans., vol. 24, no. 1, 1981, pp. 1-14.
3. Cusano, C.; and Wedeven, L. D.: The Effects of Artificially Produced Defects on the Film Thickness Distribution in Sliding EHD Point Contacts. ASME Paper 81-Lub-46, Oct. 1981.
4. Hewko, L. O.; Rounds, F. G., Jr.; and Scott, R. L.: Tractive Capacity and Efficiency of Rolling Contacts. Rolling Contact Phenomena, Joseph B. Bidwell, ed., Elsevier Publishing Co., 1962, pp. 158-185.
5. Jefferis, J. A.; and Johnson, K. L.: Sliding Friction Between Lubricated Rollers. Proc. Inst. Mech. Eng., vol. 182, no. 14, 1968, pp. 281-291.
6. Johnson, K. L.; and Tevaarwerk, J. L.: Shear Behavior of Elastohydrodynamic Oil Films. Proc. Royal Soc. London, vol. A356, 1977, pp. 215-236.
7. Bair, S.; and Winer, W. O.: Regimes of Traction in Concentrated Contact Lubrication. ASME Paper 81-Lub-16, 1981.
8. Nemlekar, P. R.; and Cheng, H. S.: Traction in Rough Elastohydrodynamic Contact. Surface Roughness Effects in Hydrodynamics and Mixed Lubrication, S. M. Rohde and H. S. Cheng, eds., ASME, 1980, pp. 173-191.
9. Tallian, T. E.: Pressure and Traction Rippling in Elastohydrodynamic Contact of Rough Surfaces. J. Lubr. Technol., vol. 96, no. 3, July 1974, pp. 398-409.
10. Wedeven, L. D.: Traction and Film Thickness Measurements Under Starved Elastohydrodynamic Conditions. J. Lubr. Technol., vol. 97, no. 2, 1975, pp. 321-329.
11. Wedeven, L. D.: Effect of Starvation on Film Thickness and Traction Under Elastohydrodynamic Rolling and Sliding Conditions. NASA TN D-8087, 1975.
12. Wedeven, L. D.; Evans, D.; and Cameron, A.: Optical Analysis of Ball Bearing Starvation, J. Lubr. Technol., vol. 93, no. 3, July 1971, pp. 349-363.
13. Foord, C. A.; et al.: Optical Elastohydrodynamics. Proc. Inst. Mech. Eng., Part 1, vol. 184, no. 28, 1969-1970, pp. 487-505.
14. Hata, H.; Nakahara, T.; and Aoki, H.: Measurement of Friction in Lightly Loaded Hydrodynamic Sliders with Striated Roughness. Surface Roughness Effects in Hydrodynamic and Mixed Lubrication, S. M. Rohde and H. S. Cheng, eds., ASME, 1980, pp. 75-92.
15. Tallian, T. E.: The Theory of Partial Elastohydrodynamic Contacts. Wear, vol. 21, 1972, pp. 49-101.
16. Whitehouse, D. J.; and Archard, J. F.: The Properties of Random Surfaces of Significance in Their Contact. Proc. Royal Soc. London, vol. A316, no. 1524, 1970, pp. 97-121.
17. Kannel, J. W.; and Tevaarwerk, J. L.: Stress Evaluations Under Rolling/Sliding Contacts. NASA CR-165561, 1981.
18. Bair, S.; and Winer, W. O.: Shear Strength Measurements of Lubricants at High Pressure. J. Lubr. Technol., vol. 101, no. 3, July 1979, pp. 251-257.
19. Bair, S.; and Winer, W. O.: A Rheological Model for Elastohydrodynamic Contacts Based on Primary Laboratory Data. J. Lubr. Technol., vol. 101, no. 3, July 1979, pp. 258-265.
20. Tevaarwerk, J. L.; and Johnson, K. L.: Influence of Fluid Rheology on the Performance of Traction Drives. J. Lubr. Technol., vol. 101, no. 3, July 1979, pp. 266-274.
21. Wilson, W. R. D.; and Sheu, S.: Viscoplastic Lubrication of Asperities. ASME Paper 81-Lub-43, 1981.

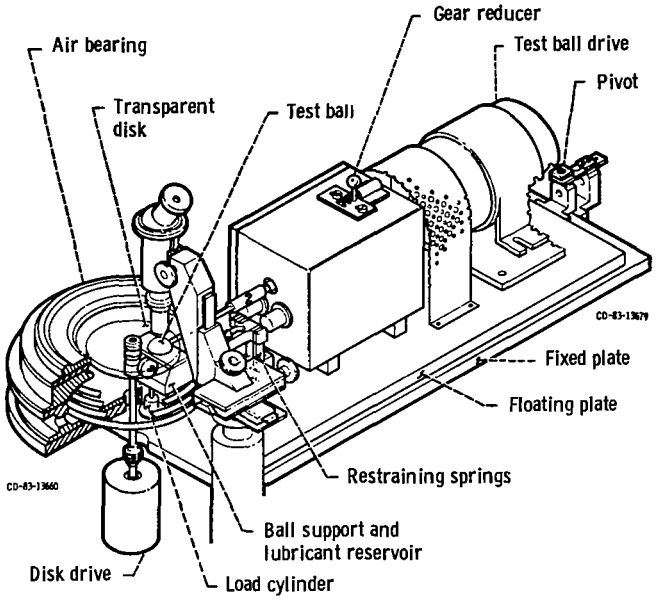

Figure 1. - Optical elastohydrodynamic lubrication test apparatus.

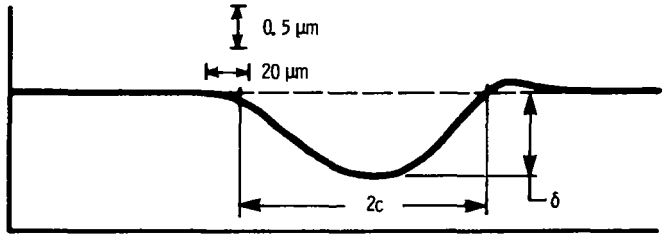

Figure 3. - Photomicrograph of small dent and stylus trace through deepest part of dent. Maximum depth, δ, 1.01 μm; one-half of largest width, c, 57.2 μm.

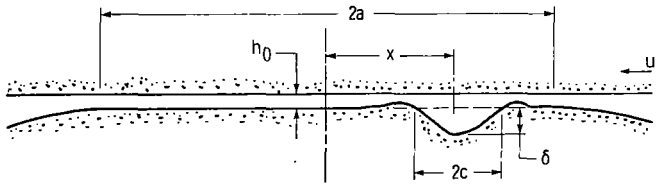

Figure 2. - Variables used to describe geometry and position of defects.

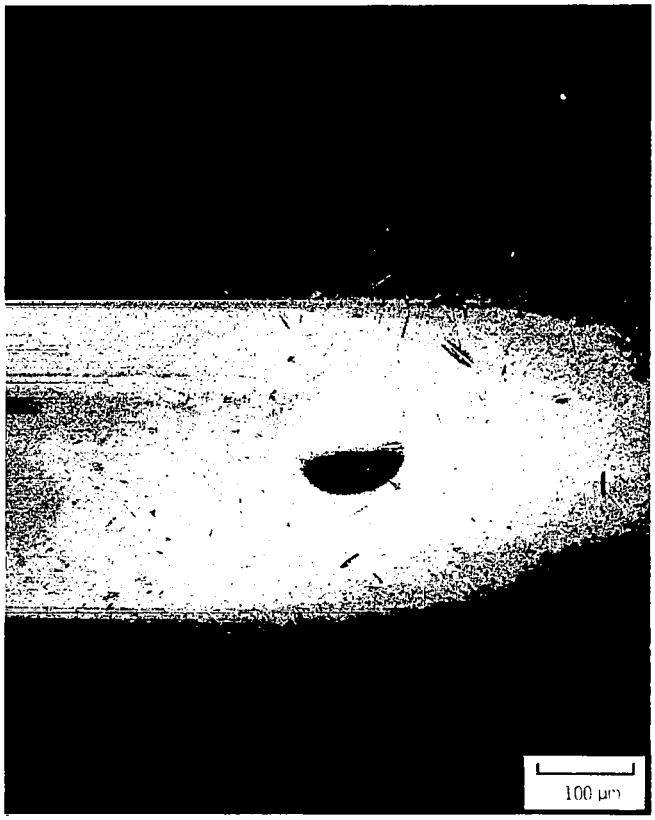

Figure 4. - Photomicrograph of large dent and stylus trace through deepest part of dent. Maximum depth, δ, 1.56 µm; one-half of largest width, c, 62.2 µm.

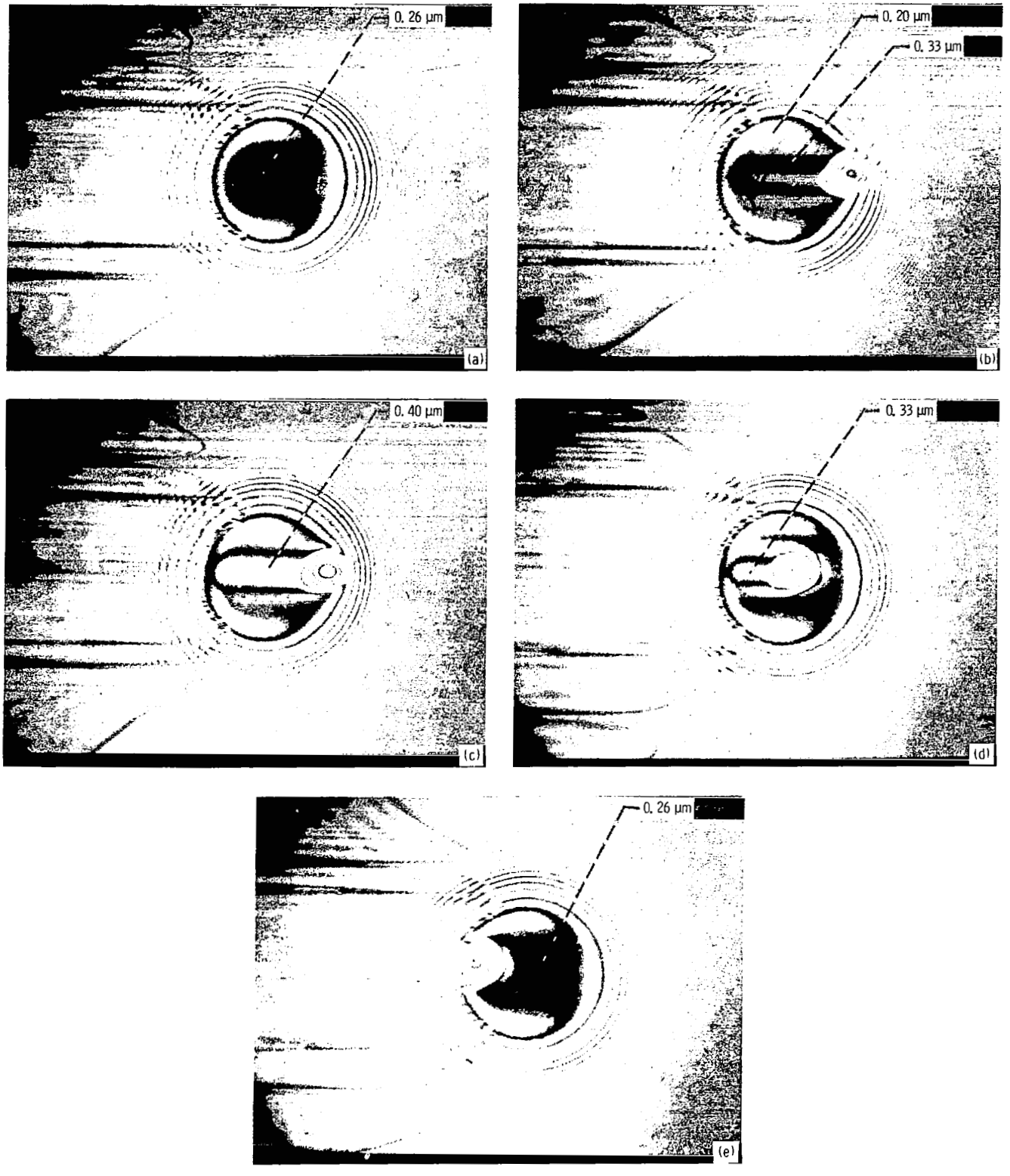

Figure 5. - Photomicrographs of interference fringes used to obtain film thickness data given in figure 6(b) for the small dent.

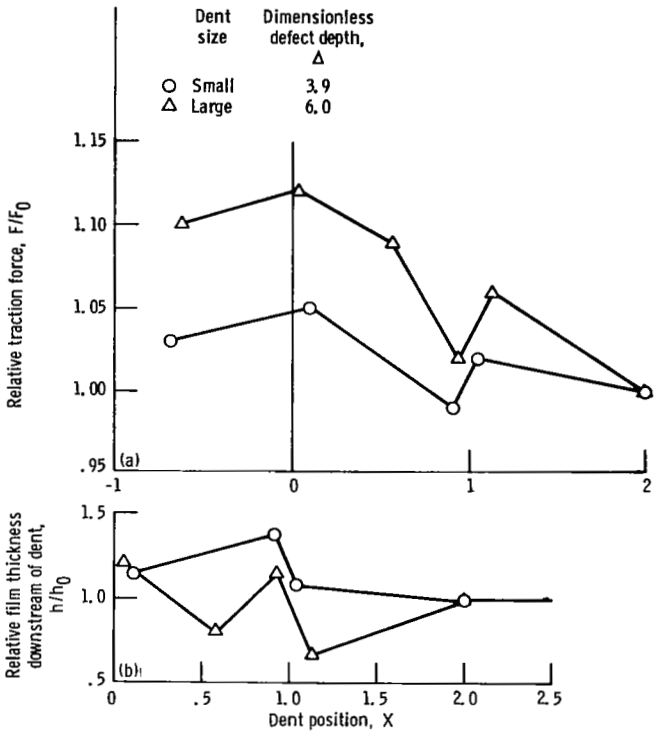

(a) Relative traction force.
(b) Relative film thickness.

Figure 6. - Relative traction and film thickness for large and small dents as a function of dent position. Disk velocity, 0.107 m/s; maximum Hertzian pressure, 1.13 GPa; temperature, 23° C; central film thickness based on smooth surfaces, h_0, 0.26 μm.

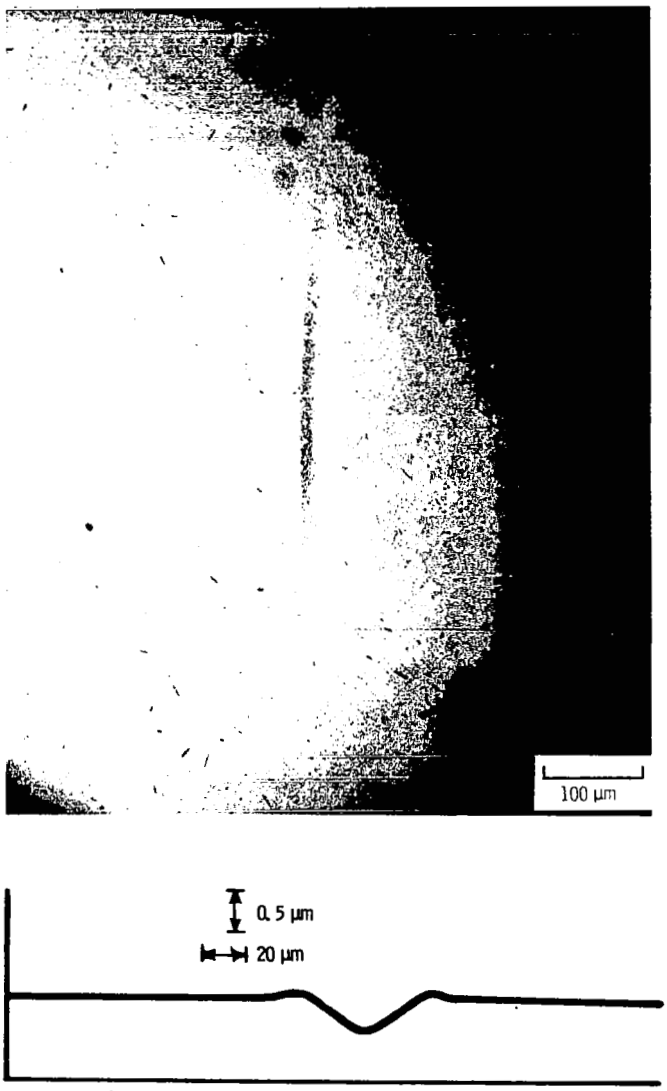

Figure 7. - Photomicrograph of transverse groove and stylus trace through deepest part of groove. Maximum depth, δ, 0.40 μm; one-half of largest width, c, 40 μm.

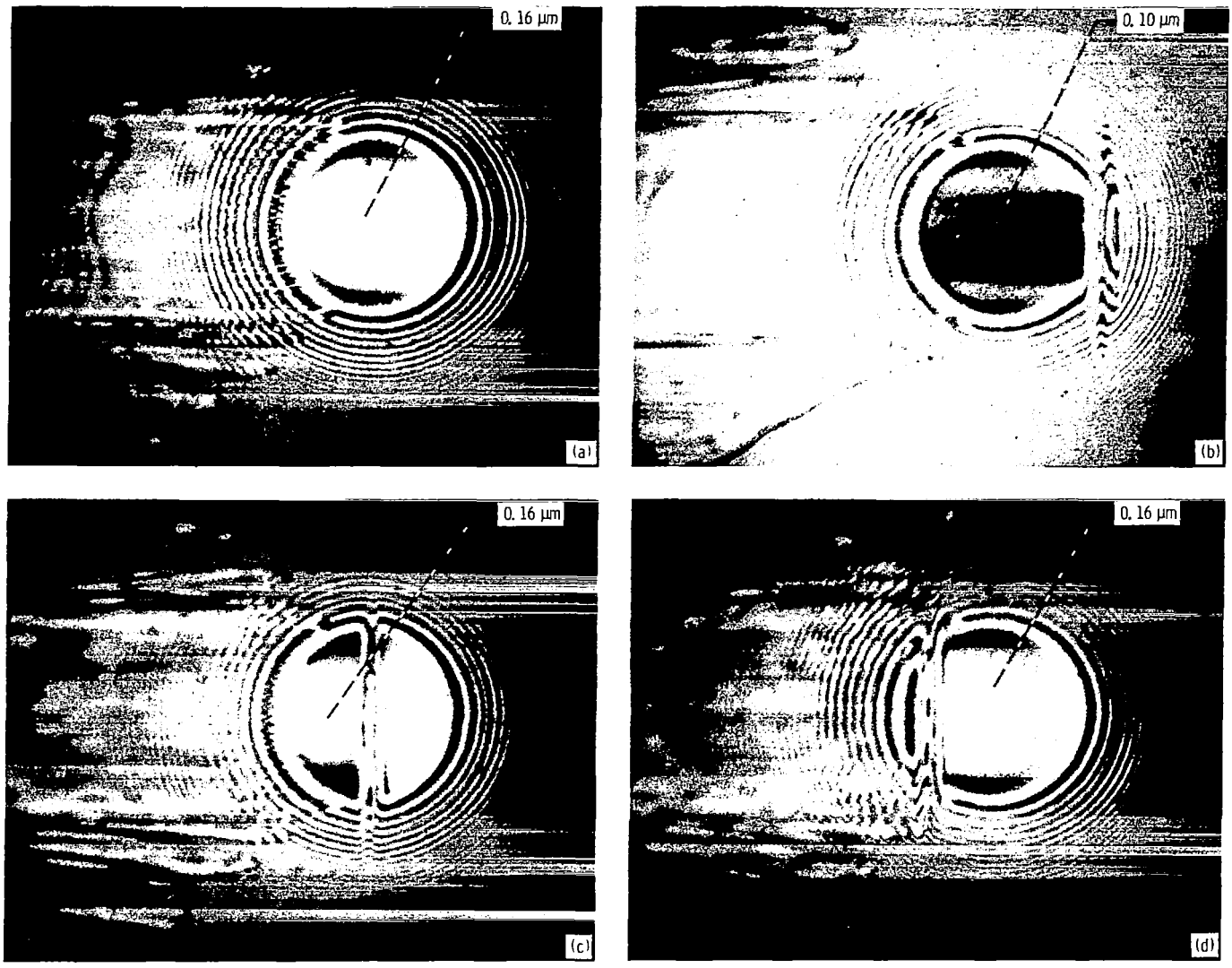

Figure 8. - Photomicrographs of interference fringes showing effect of groove location on film thickness. Central film thickness based on smooth surfaces, h_0, 0. 16 μm.

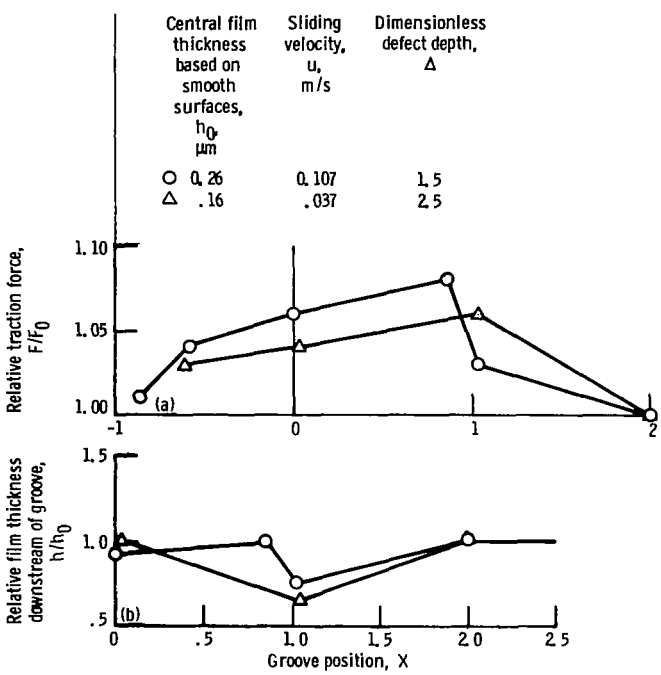

(a) Relative traction force.
(b) Relative film thickness.

Figure 9. - Relative traction force and film thickness for transverse groove as a function of groove position for two nominal film thicknesses. Maximum Hertzian pressure, 1.13 GPa.

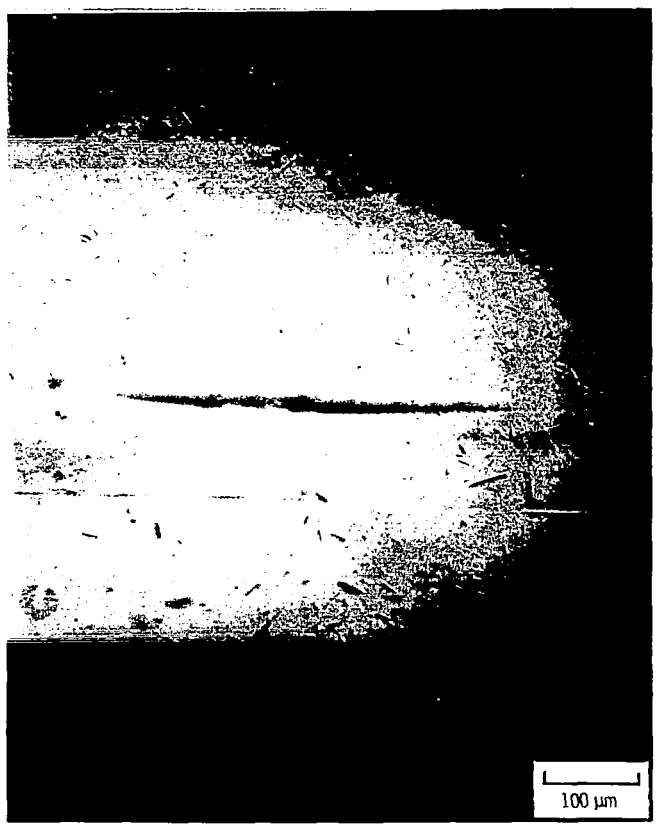

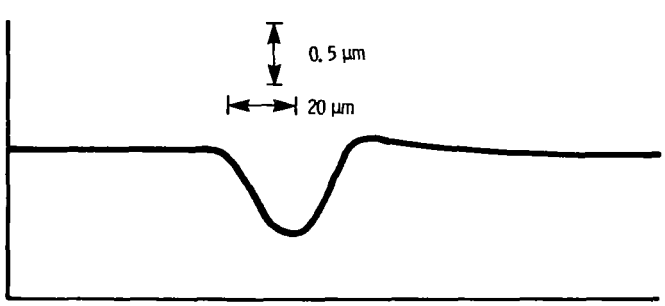

Figure 10. - Photomicrograph of longitudinal groove and stylus trace through deepest part of groove. Maximum depth, δ, 0.70 μm; one-half of largest width, c, 19.1 μm.

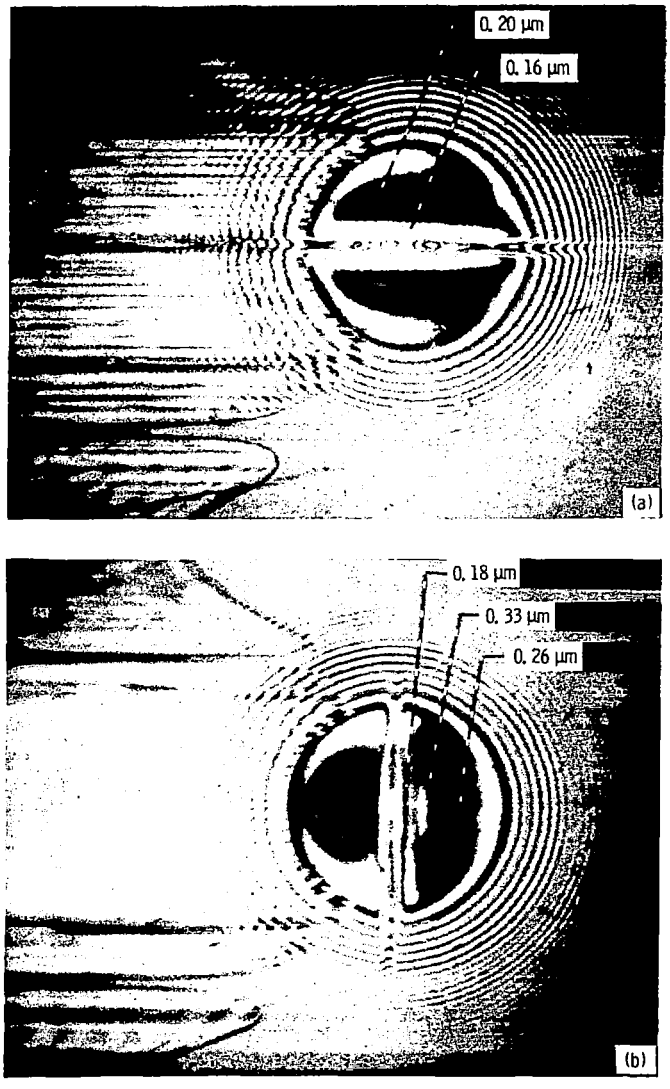

(a) Longitudinal groove.
(b) Transverse groove.

Figure 11. - Photomicrographs of interference fringes for longitudinal and transverse grooves. Central film thickness based on smooth surfaces, h_0, 0. 26 μm.

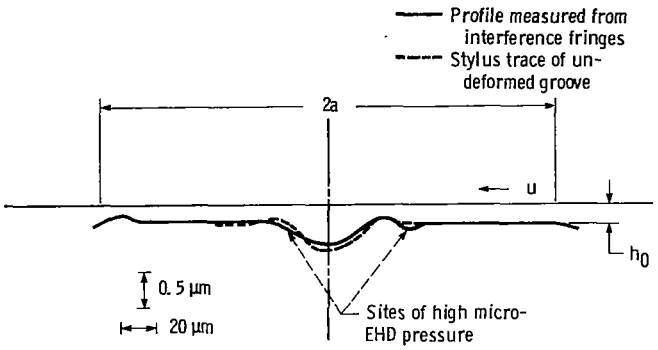

Figure 12. - Film thickness distribution for shallow transverse groove. Maximum depth, δ, 0. 40 μm; one-half of largest width, c, 40 μm; central film thickness based on smooth surfaces, h_0, 0. 26 μm; sliding velocity, u, 0. 107 m/s; maximum Hertzian pressure, 1. 13 GPa; relative traction force, F/F_0, 1. 06.

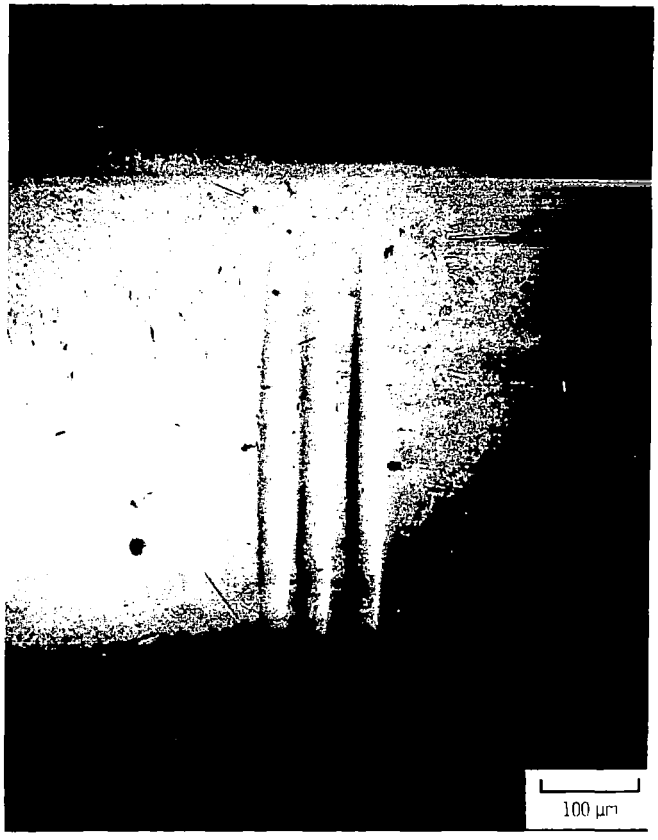

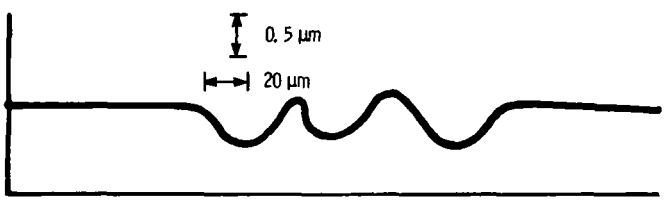

Figure 13. - Photomicrograph of three grooves and stylus trace through deepest part of grooves. Average maximum depth, δ, 0. 42 μm; average of largest widths, c, 17. 8 μm.

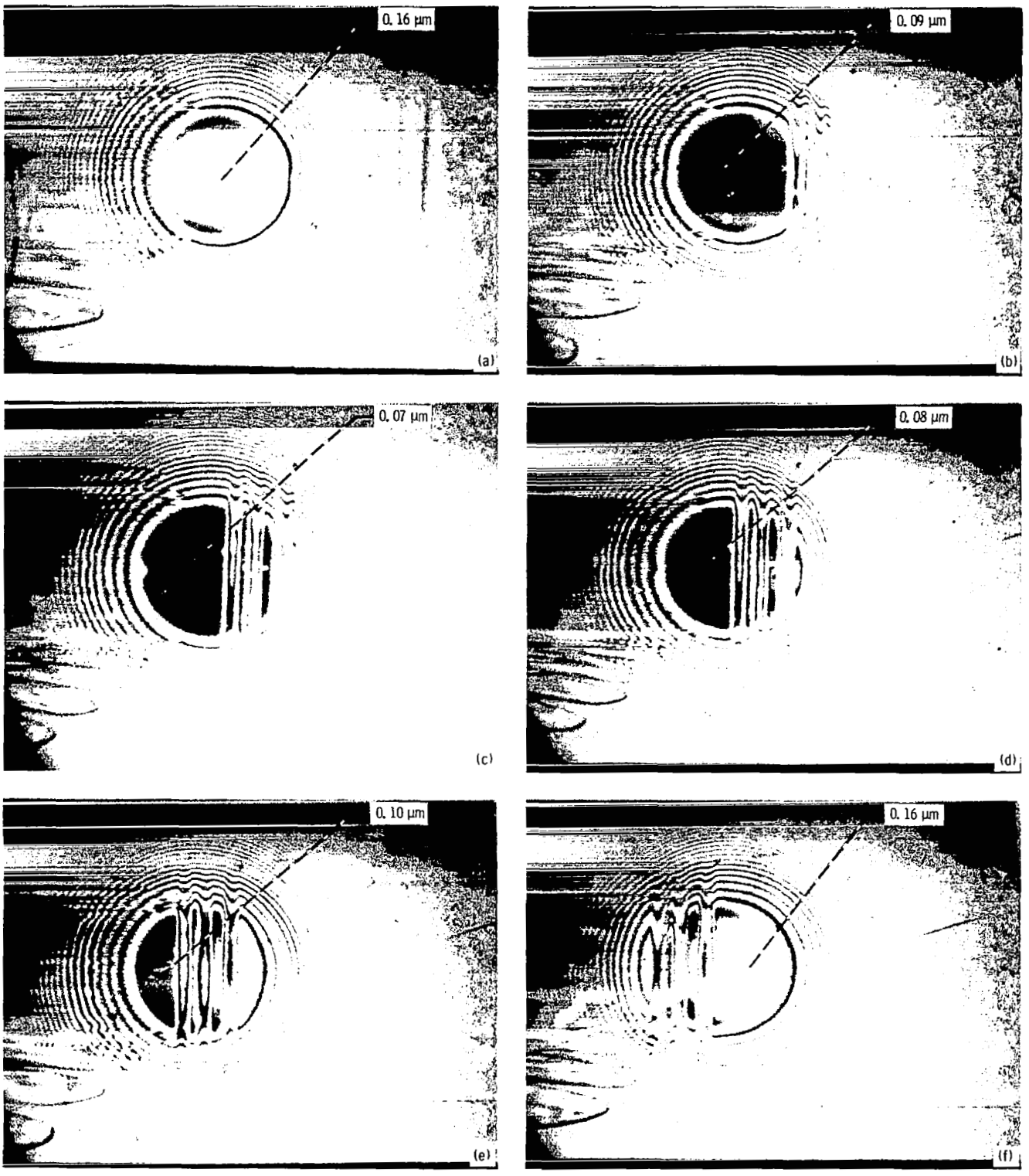

Figure 14. - Photomicrographs of interference fringes used to obtain film thickness data given in figure 15(b). Central film thickness based on smooth surfaces, h_0, 0. 16 μm.

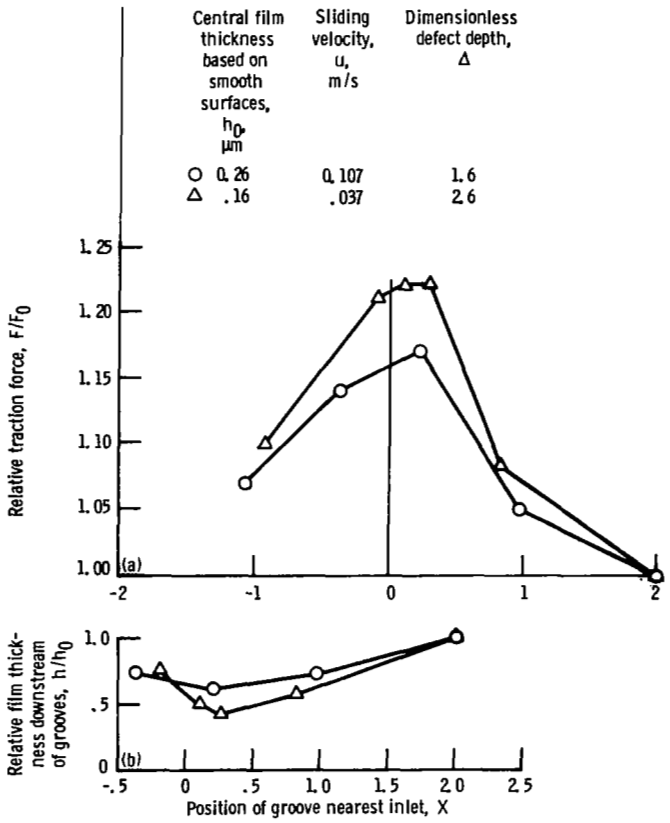

(a) Relative traction force.
(b) Relative film thickness.

Figure 15. - Relative traction force and film thickness for three parallel grooves as a function of groove position for two nominal film thicknesses. Maximum Hertzian pressure, 1.13 GPa; temperature, 23° C.

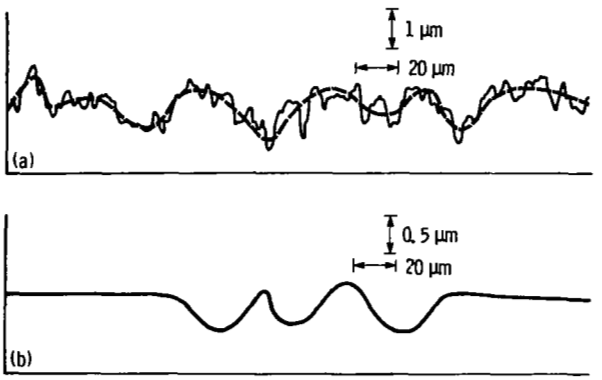

(a) Typical ground surface (ref. 16).
(b) Three grooves.

Figure 16. - Comparison of stylus traces.

1. Report No. NASA TP-2175	2. Government Accession No.	3. Recipient's Catalog No.
4. Title and Subtitle ELASTOHYDRODYNAMIC CONTACTS - EFFECTS OF DENTS AND GROOVES ON TRACTION AND LOCAL FILM THICKNESS		5. Report Date June 1983 6. Performing Organization Code 505-32-1B
7. Author(s) Lavern D. Wedeven and Cristino Cusano		8. Performing Organization Report No. E-1333 10. Work Unit No.
9. Performing Organization Name and Address National Aeronautics and Space Administration Lewis Research Center Cleveland, Ohio 44135		11. Contract or Grant No.
12. Sponsoring Agency Name and Address National Aeronautics and Space Administration Washington, D.C. 20546		13. Type of Report and Period Covered Technical Paper 14. Sponsoring Agency Code

15. Supplementary Notes
Lavern D. Wedeven, Lewis Research Center; Cristino Cusano, University of Illinois at Urbana-Champaign, Urbana, Illinois, and Summer Faculty Fellow at Lewis Research Center.

16. Abstract

Traction and film thickness were simultaneously measured under sliding elastohydrodynamic (EHD) conditions. The influence of surface topography was investigated by using simulated surfaces produced by depressing dents and grooves in highly polished steel balls. Significant changes in traction occurred depending on the orientation of the surface defects and their location with respect to the contact region. The results can be explained in terms of changes in overall film thickness and redistribution of pressure within the contact region due to micro-EHD effects. It can be concluded that the traction capability of mechanical components operating in thin-film lubrication can be enhanced particularly by surface topographical orientation perpendicular to the surface motion. Associated with the higher traction are increases in local shear stress and normal stress as well as an increase in temperature at asperity sites. It is postulated that the local surface topography can become involved in "run in" or failure initiation even without actual asperity contact.

17. Key Words (Suggested by Author(s))	18. Distribution Statement
Traction Elastohydrodynamics Surface topography	Unclassified - unlimited STAR Category 37

19. Security Classif. (of this report)	20. Security Classif. (of this page)	21. No. of Pages	22. Price*
Unclassified	Unclassified	18	A02

* For sale by the National Technical Information Service, Springfield, Virginia 22161 NASA-Langley, 1983